

Hard Contacts with Soft Gradients: Refining Differentiable Simulators for Learning and Control

Anselm Paulus^{*1} A. René Geist^{*1} Pierre Schumacher¹ Vit Musil² Georg Martius¹

¹ University of Tübingen, Germany ² Masaryk University, Czechia

[rene.geist, anselm.paulus]@uni-tuebingen.de

Abstract: Contact forces pose a major challenge for gradient-based optimization of robot dynamics as they introduce jumps in the system’s velocities. Penalty-based simulators, such as MuJoCo, simplify gradient computation by softening the contact forces. However, realistically simulating hard contacts requires very stiff contact settings, which leads to incorrect gradients when using automatic differentiation. On the other hand, using non-stiff settings strongly increases the sim-to-real gap. We analyze the contact computation of penalty-based simulators to identify the causes of gradient errors. Then, we propose DiffMJX, which combines adaptive integration with MuJoCo XLA, to notably improve gradient quality in the presence of hard contacts. Finally, we address a key limitation of contact gradients: they vanish when objects do not touch. To overcome this, we introduce Contacts From Distance (CFD), a mechanism that enables the simulator to generate informative contact gradients even before objects are in contact. To preserve physical realism, we apply CFD only in the backward pass using a straight-through-trick, allowing us to compute useful gradients without modifying the forward simulation.

Project page: <https://sites.google.com/view/diffmjx>

Keywords: Differentiable Simulation, Contact Modeling, Motion Planning, MPC, System Identification, Dexterous Manipulation.

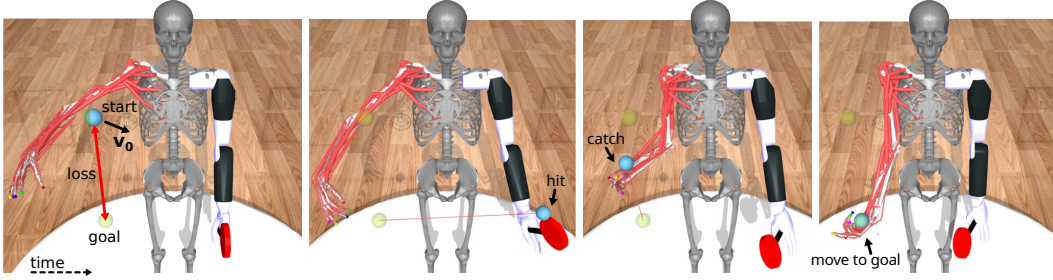


Figure 1: Autodiff-driven MPC with CFD on the bionic tennis task. Task completion requires the racket to deflect the ball towards the MyoArm with 63 muscle-tendon actuators, which then catches the ball and moves it to the goal position. **Only the distance between ball and goal is used as cost.**

1 Introduction

Simulators have proven to be an indispensable tool for synthesizing policies for robot control. Sim-to-real techniques are now the de facto standard in creating robust and performant policies for real robots [1, 2, 3, 4, 5]. Predominantly, these simulators have been used as black-box functions where policies are optimized with reinforcement learning (RL). If simulators provided informative gradients for actions and simulation parameters, a set of very powerful tools and applications would become available. We could generate policies with gradient-based MPC and RL for high-dimensional control problems that are much more sample-efficient than with classical deep RL. We could optimize

^{*} Equal contribution.

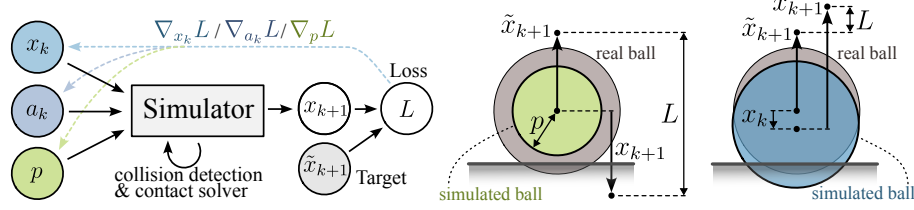


Figure 2: **Left:** Common computational graph for robot control synthesis. **Center:** If the initial ball radius p is set too small, then the gradient $\nabla_p L$ resulting from a one-step-ahead prediction is zero. **Right:** Large constraint penetration for hard contacts results in large gradients $\nabla_{x_k} L$ which aggravates the estimation of the previous state x_k .

the simulator to fit real-world observations to bridge the sim-to-real gap via gradient-based system identification. With both in place, policies for new tasks could be generated and deployed in seconds instead of hours.

What keeps us from doing it? Current simulators already provide **gradients**, but they are either **too slow, incorrect, or uninformative**. We care about sufficiently realistic simulations for real robot applications, which implies hard materials and stiff contact models. The principal source of problems is that simulators only compute a discrete approximation \tilde{F} of the continuous physics F . As a result, the gradient $\nabla \tilde{F}$ (computed using automatic differentiation) may not accurately represent the true gradient ∇F . In the sequel, gradient “correctness” refers to how closely this gradient matches the gradient of the continuous model. We show that in penalty-based simulators, which are the standard [6] in multibody physics simulation, the gradients for dynamics with contacts are incorrect to the extent that their sign can be flipped. In addition, the simulations need to be fast, so we cannot resort to infinitesimally small simulation timesteps. Previous suggestions for time-of-impact correction [7, 8] in elastic simulators do not solve the problem for penalty-based collision models, whereas softening contact dynamics or resorting to unfeasibly small timesteps do improve gradients. We propose using **adaptive timestep integrators** under the hood while keeping the fixed-timestep external interface, creating a small computational overhead but yielding correct gradients, even for hard contact cases.

Another obstacle for gradient-based optimization for policy generation and system identification is the non-informativeness of gradients about unmade contacts. For example, when a robot’s hand is not in contact with an object, then there is no gradient directing it to make contact for task facilitation. Therefore, drawing inspiration from prior works on contact-invariant optimization [9, 10], we propose **Contacts From Distance** (CFD) to address this problem. However, when done naively, introducing artificial contact forces considerably changes the simulation, resulting in a too large sim-to-real gap. In order to preserve the initial simulation, we propose using the *straight-through-trick* to only introduce CFD in the gradient computation (backward pass). We implement our changes in Mujoco XLA, the JAX [11] implementation of MuJoCo [12], and additionally fix some low-level collision routines to be truly differentiable. As a result, our implementation makes use of GPU acceleration and automatic differentiation. We show in proof-of-concept simulations that we can perform system identification and policy synthesis for collision-rich problems and hard contact in high-dimensional systems such as musculoskeletal models shown in Fig. 1.

2 Computing gradients in penalty-based simulators

As illustrated in Fig. 2, we want to use automatic differentiation to obtain the *correct* gradient of a loss functional $L(\tilde{x}_{k+1}, x_k, a_k, p)$ where the next state of the robotic system is governed by the discrete-time dynamics $x_{k+1} = \text{step}(x_k, a_k, p)$ with the state $x_k := x(t_k) = [q_k, v_k]$ at time t_k consisting of the system’s generalized position $q_k \in \mathbb{R}^{n_q}$ and velocity $v_k \in \mathbb{R}^{n_v}$, control actions $a_k \in \mathbb{R}^{n_a}$, and model parameters $p \in \mathbb{R}^{n_p}$. Typically, multi-body dynamics simulators consist of *forward dynamics model* and a *numerical integration method*. The forward dynamics govern the system’s acceleration \dot{v} via the equations of motion

$$\dot{v} = M^{-1} (\tau - c + J^\top f) \quad (1)$$

with the joint-space inertia matrix $M(q) \in \mathbb{R}^{n_v \times n_v}$, the applied forces $\tau(x, a) \in \mathbb{R}^{n_v}$, the bias force $c(x) \in \mathbb{R}^{n_v}$, the constraint space Jacobian $J(q) \in \mathbb{R}^{n_c \times n_v}$, and the constraint forces $f(x) = f_\varepsilon + f_\mathcal{F} + f_\mathcal{C} \in \mathbb{R}^{n_c}$ consisting of the equality constraint, the generalized friction, and the contact constraint forces. The Jacobian J maps joint velocity v into constraint space, whereas J^\top maps f into generalized coordinate space. The contact-free dynamics are typically derived via recursive multi-body algorithms [13, 14] while computing contact forces requires an intricate interplay of collision detection and contact force computation. Simulators typically use numerical integrators such as semi-implicit Euler and 4th-order Runge-Kutta. As we will see throughout this work, numerical integration plays a critical role for understanding how contact forces may hinder correct gradient computation. For that, we will focus on MuJoCo XLA as a concrete penalty-based simulator.

2.1 MuJoCo XLA

MuJoCo XLA (MJX) is a reimplementation of MuJoCo using the Python library JAX, which enables GPU-parallelizable gradient computation via automatic differentiation. This capability allows MJX to compute gradients of rigid-body dynamics efficiently. MuJoCo has become the de facto standard in robotics, alongside other widely used simulators such as Bullet [15], Drake [16], DiffTaichi [7] and IsaacGym [17]. The growing importance of MuJoCo within the robotics community is further evidenced by a collaborative effort between NVIDIA and Google to develop the general-purpose simulator “Newton”, built on top of the recently introduced [MuJoCo Warp](#) [18]. In order to understand where gradients computed in MJX may fail to approximate the correct ones, it is essential to first develop a solid understanding of how MuJoCo computes constraint forces.

Collision detection. A collision detector is an algorithm that, given the state x and geometry parameterizations of two bodies, returns the *signed distance* $r(x)$ between potential contact point candidates alongside with corresponding body surface normals. Collision detection is critical for contact force computation, as contacts are only considered *active* – that is, a contact point exerts contact forces – if $r(x) < 0$. For a robot simulator to be fully differentiable, it is key that the collision detector is itself differentiable. While collision detection is not the primary focus of this work, we note that obtaining reliable gradients from MJX required addressing several discontinuities in its collision detection module.

Contact force solver. When objects in a simulation come into contact, we need to determine not only where and when forces act, but also their direction and strength. MuJoCo solves this using an optimization approach inspired by Gauss’s principle [19, 20], minimizing the deviation from the unconstrained acceleration (what the system would do subject to constraint-free forces alone), while ensuring that all constraints are satisfied. Rather than solving rigid equations exactly, MuJoCo uses a softened formulation that blends two ideas: minimizing unexpected accelerations, and steering the system towards satisfying constraints using spring-damper dynamics.

The core of this approach lies in two functions: the *impedance* $d(r)$, and the *position-level reference acceleration* $h(r)$. The impedance $d(r) \in (0, 1)$ describes how strongly a constraint resists violation – it controls both how much force can be applied and how costly that force is to the solver. As illustrated in Fig. 3, the impedance $d \in (0, 1)$ is a polynomial spline function of the constraint violation r specified by the parameters $\text{solimp} = (d_o, d_w, w, \text{midpoint}, \text{power})$. The reference acceleration $h(r)$, in turn, defines how the solver aims to correct constraint violations over time, based on the velocity and position error, and given solref parameters consisting of the time constant t_c and the damping ratio ϕ_d . Internally, MuJoCo reformulates this as a convex optimization problem and solves it efficiently using a Newton method. For an in-depth description of Mujoco’s contact computation consult Suppl. B.1.

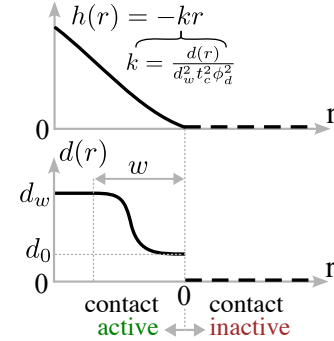


Figure 3: The position-level reference acceleration $h(r)$ and impedance $d(r)$ determine the contact force magnitudes that the solver can apply.

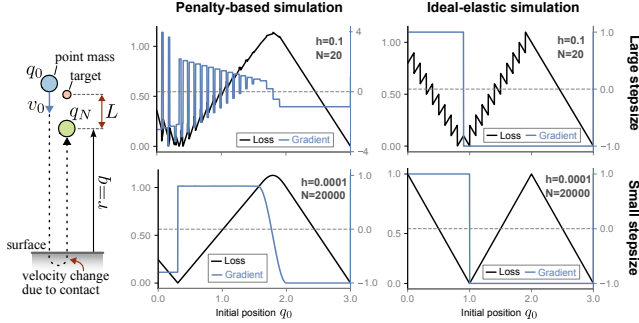


Figure 4: Toy simulation of a point mass colliding with a surface that either resorts to an ideal-elastic contact model (similar to DiffTaichi) or a penalty-based contact model (similar to MuJoCo). Loss and gradients with respect to q_0 . The loss $L = |q_N - 1|$ uses the final state q_N , which is obtained after doing N numerical integration steps starting from q_0 with $v_0 = -1$. In the penalty-based simulation, reducing h fixes the gradient oscillations, whereas for the ideal-elastic collision, reducing h does not yield correct gradients.

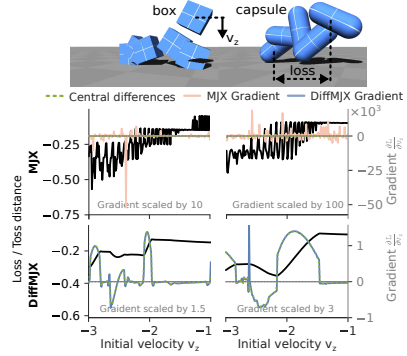


Figure 5: Simulation of geometric primitives thrown onto a surface. Contacts with stiff contact settings cause MJX’s gradients of the toss distance to deviate from central difference gradients, while DiffMJX maintains close agreement.

3 Correcting the contact gradients of penalty-based simulation

3.1 Analyzing gradient quality

To evaluate the correctness of gradients in the presence of contacts, we unroll the trajectory of several primitives bouncing against a plane and observe the final position and its gradient with respect to the initial velocity. In Fig. 5 (MJX row), we observe that the gradient is oscillating with an amplitude orders of magnitude larger than the loss.

Point mass example. To better understand this issue, we simplify the setup even further. We consider a point mass colliding with a flat surface in the absence of gravity, simulated via a minimal version of MuJoCo’s penalty-based contact model, as shown in Fig. 4 (middle column). The loss is the distance between the point’s final state and a target. Depending on the initial start height, it shows a cyclic pattern as before, which causes rapid sign flips in the gradient. Similar oscillations have been discussed in previous works [7, 8]. DiffTaichi [7] describes the “time-of-impact” (TOI) problem, showing an oscillating pattern in gradients during the ideal elastic collision. We replicate this for comparison in our toy simulator Fig. 4 (right column). These oscillations arise from time-discretization errors in ODE integration that also affect penalty-based simulators, but have to be addressed differently.

TOI correction does not fix gradients for penalty-based simulators, but small stepsizes do. For an ideal elastic collision, the ODE is piecewise linear, and at the contact, the velocity is inverted (see also Figure S4 in the Appendix). The TOI approach [7] dynamically splits the ODE into two linear segments at the time of contact, thereby eliminating the discretization error and yielding correct gradients. In penalty-based simulation, the ODE is also linear before and after the collision, but is non-linear and with variable stiffness over the time of the collision. Therefore, it cannot be easily divided into large linear segments. A possible solution would be to reduce the stepsize until the discretization error decreases enough. This is also confirmed in our toy simulator in Fig. 4: Reducing the stepsize in the penalty-based simulation eventually yields correct gradients, whereas for ideal elastic collision, the gradients remain incorrect.

Unfortunately, simply reducing the step size is not a practical solution, as it necessitates extremely small steps that substantially increase the computational and memory demands of gradient computation. This trade-off raises a critical question: *Can we retain realistic contacts while maintaining practical simulation speeds?*

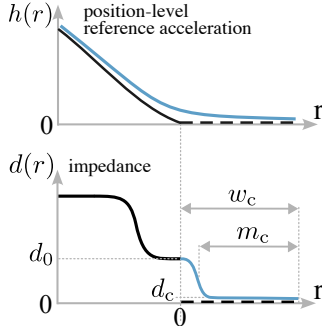


Figure 6: Contacts from distance (CFD): To let MuJoCo create small contact forces between non-colliding objects, reference acceleration $h(r)$ and impedance $d(r)$ are adjusted to be nonzero for positive signed distances $r > 0$.

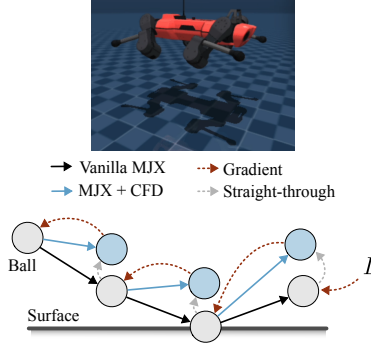


Figure 7: **Top:** Applying contact forces for $r > 0$ in the forward pass of the simulation causes a robot to hover. **Bottom:** The straight-through-trick is used to replace the original MJX derivative with the derivative of MJX + CFD, evaluated at the unaltered trajectory.

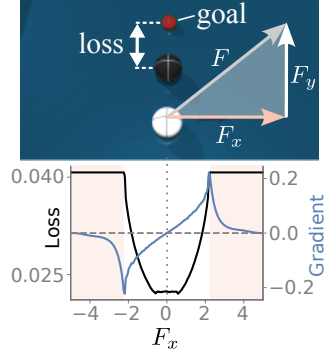


Figure 8: Billiard simulation. **Top:** Force F acts on the white ball to minimize the loss. **Bottom:** Despite the loss derivative being zero if the balls do not collide, DiffMJX with CFD provides informative gradient information.

3.2 Adaptive stepsize integration: Numerical precision on demand

A standard methods for integrating ODEs with variable stiffness are *adaptive integrators*. The idea behind adaptive stepsize integration is simple: Two numerical integrators of different order compute the next state. Their difference provides an estimate of the error. If the error is smaller than a given threshold, the step is accepted, otherwise the step is rejected and the procedure is repeated with a different stepsize chosen by a feedback controller. For further details on the rich history of adaptive stepsize integration, see e.g. [21, 22, 23, 24]. We use Diffirax [25] for efficient numerical integration in JAX, taking advantage of its solver flexibility and enhanced backpropagation modes. We extend it to integrate quaternions and stateful actuators seamlessly and make Diffirax compatible with MJX. Further details are provided in Suppl. B.2.

Resolving problems of Collision Detection. Using an adaptive integrator with MJX eliminates oscillations in the bounce example. However, gradients for some object primitives (capsule, cylinder, box) experience offsets due to non-differentiable operations in the collision detector arising from discrete case distinctions. We smoothened them with standard proxies, leading to results in the bottom row of Fig. 5, where analytical gradients nearly match central differences. Henceforth, we refer to MJX with the Diffirax integrator and smoothened collision detection as DiffMJX.

4 Contact force gradients from a distance

We can now compute the correct gradients of the dynamics. However, are these gradients also *informative*? For example, consider a simulated billiard table setup as shown in Fig. 8. The white ball should be shoot to hit the black ball and make it reach the target. We are exerting a force F onto the white ball in the first timestep and would like to optimize this force to minimize the distance L between the black ball and the target. As long as the balls collide, MJX with adaptive integration yields informative gradients $\nabla_F L$. However, if F does not cause the balls to touch, then $\nabla_F L$ is zero and therefore uninformative for optimization. Therefore, we propose *contacts from distance* (CFD), a method for computing contact forces for positive signed distances r in penalty-based simulation to yield informative gradients even if objects are not in contact.

Creating artificial contact forces from a distance. As discussed in Suppl. 2, the magnitude of contact forces in MuJoCo is determined by the impedance $d(r)$ and position-level reference acceleration $h(r)$. To enable the solver to apply CFD, we can augment $d(r)$ as depicted in Fig. 6. Here, we do not alter $d(r)$ for $r < 0$, but instead extend $d(r)$ for $r > 0$. This continuation is parametrized by *solimp-CFD* parameters $(d_c, d_0, w_c, m_c, p_c)$. By default, the curve smoothly continues MuJoCo’s impedance at d_0 and tapers off to $d_c = 0$ to ensure smooth differentiability. The CFD width w_c specifies the distance for which artificial contact forces are generated and, in our experiments, has been varied between 1 cm and 1 m. Moreover, we soften the reference acceleration $h(r)$ by replacing the ReLU function on the signed distance with a softplus (Fig. 6). This yields modified contact forces f_{CFD} , and hence the modified ODE $\dot{v}_{\text{CFD}} = M^{-1}(\tau - c + J^\top f_{\text{CFD}})$.

Designing a surrogate gradient estimator. CFD provides contact gradients for positive signed distances at the expense of physical realism. As shown in Fig. 7 (top), naive simulation with CFD results in floating objects. In this example, CFD can be seen as introducing a compliant layer mimicking a soft foam mat of thickness w_c being placed atop the actual surface. In turn, the quadrupedal robot appears to hover above the surface. As significantly altering simulation realism is not an option, we are faced with the question: *Can CFD be used to obtain informative contact gradients without affecting simulation realism?*

To positively answer this question, we propose a simple idea: we keep the forward computation (vanilla MJX or DiffMJX), but enable CFD only in a simulation used for gradient computation via automatic differentiation. This is achieved by a variation of the straight-through-trick applied to the forward dynamics model, as detailed in Suppl. B.3. The resulting procedure is illustrated in Fig. 7 (bottom). Note that this approach requires the simulator’s forward pass to be computed twice. However, the gradient, which typically dominates the computational cost, is still only evaluated once.

Revisiting the billiard example from the beginning of this section (Fig. 8), we see that by using the straight-through-trick, DiffMJX computes both the correct loss as well as gradients pointing towards the loss minimum despite the balls not being in contact.

5 Evaluation

5.1 System Identification

Parameter identification in the presence of hard contacts remains a laborious task. If contacts are hard, even learning the dynamics of a cube requires impractical amounts of data for “naive” neural network regression [27]. In comparison, penalty-based simulators can capture hard contacts, but the lack of correct gradients hinders efficient parameter estimation [28]. Therefore, recent work introduced intricate analytical pipelines for cube geometry estimation [26, 29] and graph-based networks for learning contact dynamics [30]. In what follows, we use the same real-world data as used in [26, 29, 30]. We demonstrate that DiffMJX with CDF enables simulator parameter estimation via standard gradient-based optimization.

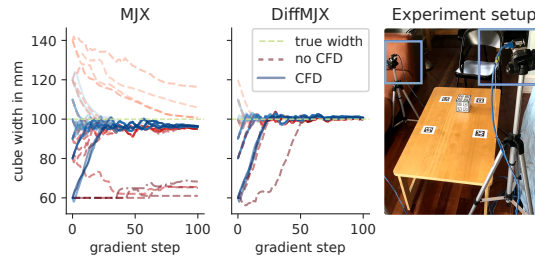


Figure 9: **Left:** Estimation of a cube’s side length in MJX via gradient descent using multi-step ahead predictions. **Right:** Experimental setup for collecting cube toss data. Image adapted from [26].

Dataset and training setup. We use the Contactnets dataset [26] which consists of 550 trajectories of an 10 cm acrylic cube that has been repeatedly tossed onto a wooden table. For training, trajectories are split into segments of length five such that the simulator is tasked to unroll four future steps starting from the initial state. Each segment and its prediction is fed to an L_2 loss whose gradient is used for gradient-based optimization using Adam [31]. For systems with stiff dynamics, we favor

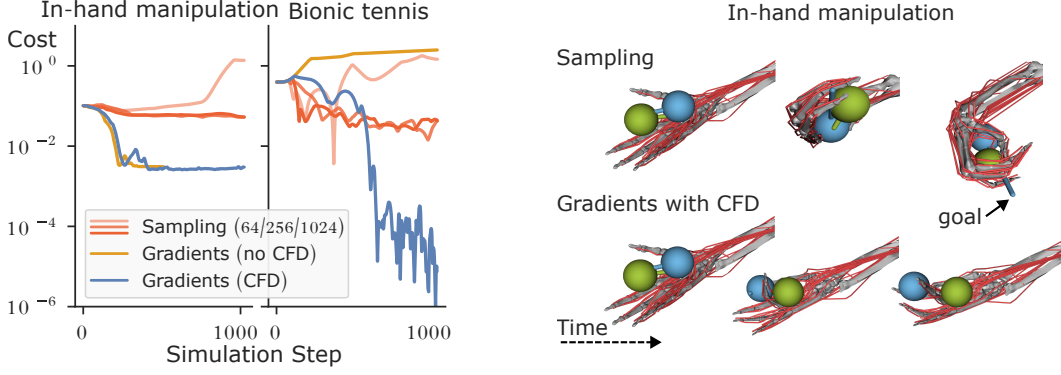


Figure 10: **Left:** Simulation cost evolution of gradient-based MPC, with and without contacts from distance (CFD), vs sampling-based MPC. The number for sampling indicates the number of samples used per planning step. Sampling has difficulties solving the dexterous in-hand manipulation task; gradients without CFD cannot solve the bionic tennis task. **Right:** Rendering of sampling-based MPC (1024 samples) vs gradient-based MPC with CFD on in-hand manipulation task. The goal is to swap the balls; the MyoHand model is actuated by 39 muscle-tendon units.

multi-step-ahead predictions over one-step-ahead predictions, as they capture the cumulative effects of prediction errors over time. This setup enables a fairer analysis of MJX without CFD, as even for too small side length estimates, future state predictions can make contact to inform the optimization.

Training results. The training results are shown in Fig. 9. Surprisingly, the refined version of MJX and MJX with CFD already achieve good estimation results with an error of around 5% relative to the ground-truth. If the side length is initialized at 60 mm or 140 mm, training either stalls fully or convergence is severely limited for MJX. The incorporation of CFD into MJX addresses convergence issues arising from poor initial parameters, while the integration of adaptive integration via DiffMJX significantly enhances estimation accuracy. DiffMJX improves estimation accuracy by dynamically adjusting the time steps during collisions, thereby mitigating time discretization errors. Further details and parameter estimation experiments are provided in Suppl. C.2. To the best of our knowledge, we are the first to demonstrate parameter estimation of real-world cube dynamics using an automatically differentiable penalty-based simulator. While this represents a promising step forward, further experimentation is necessary to fully characterize the scope and limitations of this approach.

5.2 Model Predictive Control

Next, we conduct experiments on gradient-based model-predictive control. We use a simple MPC loop in which, at every plan step, we refine a sequence of controls over a 256-step horizon. In the gradient-based planner, we compute gradients by backpropagating the differentiable cost computed on the rollout of the current plan through the MJX simulator. The plan is then iteratively optimized using the Adam optimizer with a learning rate of 0.01 for 32 iterations. Finally, the resulting plan is executed for 16 steps in simulation, after which the planning procedure is repeated with the previous plan as a warm start. As a simple baseline, we include a version of the predictive sampling planner from Mujoco MPC [32], which at every plan step samples $k = \{64, 256, 1024\}$ trajectories, and executes the lowest-cost plan. We significantly improved the performance of this planner for the muscular systems by resorting to brown noise [33] for sampling.

Models. All our MPC experiments revolve around the muscle-tendon models provided by MyoSuite [34, 35]. Models include the MyoHand modified from the MyoChallenge 2022, which is comprised of 29 bones, 23 joints, and 39 muscle-tendon units. We also use a bionic model modified from the MyoChallenge 2024, which is comprised of the MyoArm with 27 degrees of freedom and 63 muscle-tendon units, and the simulated modular prosthetic limb with 26 degrees of freedom and 17 motor control units.

Dexterous in-hand manipulation: Determining crucial components in the MPC loop. First, we consider an in-hand manipulation task, where the goal is to swap two balls in the MyoHand. The cost is given by the Euclidean distance between each of the balls and the respective target location, fixed in the frame of the hand.

The results are reported in Fig. 10. We find that gradient-based MPC can reliably solve this task, in contrast to the sampling-based planner. Overparameterization in the muscle-tendon model with at least two muscles per joint benefits the gradient-based planner by helping escape local minima, similar to its role in optimizing overparametrized neural networks. In contrast, RL and sampling-based planners struggle with scaling in overparametrized higher-dimensional systems [36]. First-order methods using differentiable simulation should be able to tackle more complex control problems.

Notably, this task does not require distant contacts because hand-ball interactions are frequent due to gravity. Moreover, we identify two crucial components of the gradient-based MPC loop: First is gradient clipping, which is important as the scale of gradients changes massively in the presence of contacts. This technique has also been reported to be effective in previous works on differentiable simulation [37, 38]. Second, we store the rollout cost of all gradient iterations and select the one with minimal cost. This is important as the cost landscape is highly non-convex, which is reflected in the non-monotonic cost evolution between the iterations of a planning step.

Bionic tennis: Using CFD to solve complex control tasks with minimal task supervision. Finally, we test a more complex custom bionic tennis task on the bionic model. The task is to move a ball that is initially moving sideways to a target location below. This can be achieved by bouncing it back using a racket that is statically welded to the prosthetic hand, and then catching it at the target location with the muscle hand. In this task, *the only cost supervision is the Euclidean distance of the ball to the target*, the complicated sequential movement has to be discovered purely from this signal.

We report our findings in Fig. 10, see Fig. 1 for a rendering. By design, the task initialization is such that the ball misses both hands, hence this task is not solvable by purely gradient-based MPC using vanilla MJX. On the other hand, we observe that adding the contacts from the distance mechanism allows solving this task. The sampling-based planner is a strong baseline in this task and gets very close to solving it. Initially bouncing the ball back to the target only requires controlling the prosthetic arm which is relatively low-dimensional, hence the sampling-based planner achieves this part easily. However, as seen in the in-hand manipulation task, it struggles with precise control of the high-dimensional MyoHand.

6 Conclusion

In this work, we tackle the challenge of inaccurate gradient computation in differentiable penalty-based simulators, such as MuJoCo XLA (MJX), arising from hard contact dynamics. Through a 1D toy example, we demonstrate that these errors are a consequence of time-discretization and can be mitigated by reducing the integration stepsize. While reducing the stepsize improves gradient accuracy, it comes at the cost of increased simulation time and GPU memory usage. To address these limitations, we introduced DiffMJX, which is a combination of MJX with the adaptive numerical integration library DiffraX. This approach enables the use of adaptive time integration to reduce discretization errors while significantly reducing memory overhead through checkpointing. To further improve differentiability in contact-rich environments, we smoothen MJX’s collision detection pipeline, enabling accurate gradient computation of MuJoCo’s basic shape primitives for enabling stiff contact settings. Complementing DiffMJX, we propose Contacts from Distance (CFD), a technique that improves gradient utility by introducing small virtual contact forces between near-interacting bodies, without affecting the forward simulation. CFD is implemented via the straight-through-trick. We validate these contributions in a real-world system identification experiment, where DiffMJX successfully estimates the geometric parameters of a cube via simple gradient descent. Moreover, this work is the first to demonstrate that automatic differentiation with CFD can outmatch sample-based predictive planning in bionic dexterous manipulation tasks.

7 Limitations

7.1 Computational cost of DiffMJX

DiffMJX increases the computational cost of MJX depending on the integrator settings. A detailed analysis of DiffMJX computational cost is given in Figure S6. If an adaptive integrator is chosen, then the computational cost may notably increase as many more steps are taken during simulation. However, as we show that achieving well-behaved gradients in the presence of hard contacts requires a sufficiently small stepsize, this is a necessary price to pay. The alternative is to reduce the native fixed MJX stepsize, which will require many more steps when the stiffness of the ODE changes a lot due to collision events. Notably, there is a non-negligible increase in JIT compilation time when using Difffrax, as the program is compiled for the maximum number of ODE steps that is set by the user. That said, thanks to Difffrax’s advanced techniques for checkpointing, DiffMJX memory consumption is significantly reduced compared to MJX.

Through Difffrax, DiffMJX provides a whole suite of additional tuning knobs that can be used to improve gradient computation. The most important parameter by far is the integrator’s error tolerances, which directly determine to what extent discretization errors cause oscillations in the gradient signal. Ideally, we want to choose the smallest error tolerance that provides sufficiently good gradients to keep the computational footprint small. However, this error tolerance depends on the stiffness of the simulation, aka the hardness of contacts and joint limits. The error tolerance is an additional hyperparameter that requires tuning.

7.2 Impact of number of contacts on CFD

The documentation of MuJoCo XLA¹ advises to use meshes with 200 vertices or fewer due to computational limitations on the current implementation of collision detection. If MJX is used with CFD, then every contact is added to the contact solver for which $r < w_c$. In turn, for dense meshes and large w_c , computation can become prohibitively large. The parameter w_c can be made arbitrarily small such that, in its limit for $w_c = 0$, we retain vanilla MJX with our improvements on the differentiability of the collision detector.

While gradients computed with CFD enable controller synthesis for highly-dimensional systems such as muscular robots, it can only do so effectively if the number of contacts remains small. That said, for in-hand manipulation tasks and robot locomotion tasks, the number of objects colliding at one instance is usually small enough to render CFD a useful tool for easing optimization with penalty-based simulators.

7.3 System Identification

For the very large initial cube side length initial value of 140 mm, DiffMJX saw a significant drop in computation speed forcing us to abort these runs. This is not surprising as penetrations amounting to 40% of the total cube’s width cause large contact forces that significantly stiffen the ODE. In Appendix C.2, we reduce the integration error tolerance which allowed optimization to converge even for large initial parameters. Alternatively, one could speed up training for these too large geometry parameter initializations by first using a soft impedance that during training becomes annealed to become increasingly stiff.

In principle, our implementation of DiffMJX enables gradient computation with respect to any differentiable simulator parameter, including the cube’s mass and inertia, as well as contact model parameters such as *solref* and *solimp*. However, since gradient descent is a local optimization method, it is susceptible to convergence to local minima as shown in Appendix C.2. The results shown in Fig. 9 converged reliably when the simulated cube’s mass was set to the ground-truth value and the contact parameters were tuned to somewhat resemble the real-world motion. In scenarios where no

¹<https://mujoco.readthedocs.io/en/stable/mjx.html#mjx-the-sharp-bits>

prior knowledge of simulator parameters is available, one likely needs to combine DiffMJX with global optimization methods such as randomly sampling initial simulator parameters.

7.4 Gradient-based vs sampling-based MPC

In general, gradient computation with MJX via autodifferentiation is considerably slower than running only the forward simulation. This makes zeroth-order methods such as predictive sampling favorable whenever the task can be solved with them, as the runtime is much lower. However, sampling suffers from the curse of dimensionality, whereas gradients scale to extremely high-dimensional control problems.

For MPC, our CFD mechanism tends to be effective when the object needs to be pushed in a specific direction by the hand, but it performs poorly in grasping tasks. This limitation arises because, at a distance, the cumulative force arising from the hand’s CFDs conglomerate into a force that pushes objects away. However, the gradient does not encode the possibility of grasping, as this signal only emerges when the object is inside the hand. Fundamentally, this issue reflects the non-convex nature of the optimization landscape.

However, we do not believe that this is a problem that should be solved using a CFD mechanism; rather, in such tasks, the best approach would be to combine CFD with sampling to overcome the non-convexity while maintaining the favorable scaling of gradients with dimensionality.

Acknowledgements

The authors thank Onur Beker, Thomas Rupf, and Nico Gürtler for providing valuable feedback.

This work was supported by the ERC - 101045454 REAL-RL and the German Federal Ministry of Education and Research (BMBF) through the Tübingen AI Center (FKZ: 01IS18039B). Georg Martius is a member of the Machine Learning Cluster of Excellence, EXC number 2064/1 – Project number 390727645.

References

- [1] J. Tan, T. Zhang, E. Coumans, A. Iscen, Y. Bai, D. Hafner, S. Bohez, and V. Vanhoucke. Sim-to-real: Learning agile locomotion for quadruped robots. In *Proceedings of Robotics: Science and Systems*, Pittsburgh, Pennsylvania, June 2018. doi:10.15607/RSS.2018.XIV.010.
- [2] J. Lee, J. Hwangbo, L. Wellhausen, V. Koltun, and M. Hutter. Learning quadrupedal locomotion over challenging terrain. *Science Robotics*, 5(47):eabc5986, Oct. 2020. doi:10.1126/scirobotics.abc5986.
- [3] O. M. Andrychowicz, B. Baker, M. Chociej, R. Józefowicz, B. McGrew, J. Pachocki, A. Petron, M. Plappert, G. Powell, A. Ray, J. Schneider, S. Sidor, J. Tobin, P. Welinder, L. Weng, and W. Zaremba. Learning dexterous in-hand manipulation. *The International Journal of Robotics Research*, 39(1):3–20, Jan. 2020. ISSN 0278-3649. doi:10.1177/0278364919887447.
- [4] I. Radosavovic, T. Xiao, B. Zhang, T. Darrell, J. Malik, and K. Sreenath. Real-world humanoid locomotion with reinforcement learning. *Science Robotics*, 9(89):eadi9579, Apr. 2024. doi:10.1126/scirobotics.adi9579.
- [5] C. Li, M. Vlastelica, S. Blaes, J. Frey, F. Grimmering, and G. Martius. Learning agile skills via adversarial imitation of rough partial demonstrations. In *Proceedings of the 6th Conference on Robot Learning (CoRL)*, Dec. 2022.
- [6] E. Todorov, T. Erez, and Y. Tassa. MuJoCo: A physics engine for model-based control. In *2012 IEEE/RSJ International Conference on Intelligent Robots and Systems*, pages 5026–5033, Oct. 2012. ISSN: 2153-0866.
- [7] Y. Hu, L. Anderson, T.-M. Li, Q. Sun, N. Carr, J. Ragan-Kelley, and F. Durand. DiffTaichi: Differentiable programming for physical simulation. In *International Conference on Learning Representations*, 2020.
- [8] C. Schwarke, V. Klemm, J. Tordesillas, J.-P. Sleiman, and M. Hutter. Learning quadrupedal locomotion via differentiable simulation. *arXiv preprint arXiv:2404.02887*, 2024.
- [9] I. Mordatch, E. Todorov, and Z. Popović. Discovery of complex behaviors through contact-invariant optimization. *ACM Transactions on Graphics (ToG)*, 31(4):1–8, 2012.

- [10] I. Mordatch, Z. Popović, and E. Todorov. Contact-invariant optimization for hand manipulation. In *Proceedings of the ACM SIGGRAPH/Eurographics symposium on computer animation*, pages 137–144, 2012.
- [11] J. Bradbury, R. Frostig, P. Hawkins, M. J. Johnson, C. Leary, D. Maclaurin, G. Necula, A. Paszke, J. VanderPlas, S. Wanderman-Milne, and Q. Zhang. JAX: composable transformations of Python+NumPy programs, 2018. URL <http://github.com/google/jax>.
- [12] E. Todorov. Convex and analytically-invertible dynamics with contacts and constraints: Theory and implementation in mujoco. In *2014 IEEE International Conference on Robotics and Automation (ICRA)*, pages 6054–6061. IEEE, 2014.
- [13] R. Featherstone. Rigid body dynamics algorithms. 2014.
- [14] K. M. Lynch and F. C. Park. *Modern robotics*. Cambridge University Press, 2017.
- [15] E. Coumans and Y. Bai. Pybullet, a python module for physics simulation for games, robotics and machine learning. <http://pybullet.org>, 2016–2021.
- [16] R. Tedrake and the Drake Development Team. Drake: Model-based design and verification for robotics, 2019. URL <https://drake.mit.edu>.
- [17] J. Liang, V. Makoviychuk, A. Handa, N. Chentanez, M. Macklin, and D. Fox. Gpu-accelerated robotic simulation for distributed reinforcement learning, 2018.
- [18] T. Howell. Mujoco warp (mjwarp). https://github.com/google-deeppmind/mujoco_warp, March 2025. NVIDIA GPU Technology Conference (GTC).
- [19] C. F. Gauß. Über ein neues allgemeines Grundgesetz der Mechanik. *Journal für die reine und angewandte Mathematik*, 4:232–235, 1829.
- [20] F. E. Udwardia. The general gauss principle of least constraint. *Journal of Applied Mechanics*, 90(11): 111006, 2023.
- [21] E. Hairer, S. Nørsett, and G. Wanner. *Solving Ordinary Differential Equations I Nonstiff Problems*. Springer, Berlin, second revised edition edition, 2008.
- [22] E. Hairer and G. Wanner. *Solving Ordinary Differential Equations II Stiff and Differential-Algebraic Problems*. Springer, Berlin, second revised edition edition, 2002.
- [23] G. Söderlind. Automatic control and adaptive time-stepping. *Numerical Algorithms*, 31:281–310, 2002.
- [24] G. Söderlind. Digital Filters in Adaptive Time-Stepping. *ACM Transactions on Mathematical Software*, 20(1):1–26, 2003.
- [25] P. Kidger. *On Neural Differential Equations*. PhD thesis, University of Oxford, 2021.
- [26] S. Pfrommer, M. Halm, and M. Posa. Contactnets: Learning discontinuous contact dynamics with smooth, implicit representations. In *Conference on Robot Learning*, pages 2279–2291. PMLR, 2021.
- [27] M. Parmar, M. Halm, and M. Posa. Fundamental challenges in deep learning for stiff contact dynamics. In *2021 IEEE/RSJ International Conference on Intelligent Robots and Systems (IROS)*, pages 5181–5188. IEEE, 2021.
- [28] B. Acosta, W. Yang, and M. Posa. Validating robotics simulators on real-world impacts. *IEEE Robotics and Automation Letters*, 7(3):6471–6478, 2022.
- [29] B. Bianchini, M. Halm, and M. Posa. Simultaneous learning of contact and continuous dynamics. In *Conference on Robot Learning*, pages 3966–3978. PMLR, 2023.
- [30] K. R. Allen, T. L. Guevara, Y. Rubanova, K. Stachenfeld, A. Sanchez-Gonzalez, P. Battaglia, and T. Pfaff. Graph network simulators can learn discontinuous, rigid contact dynamics. In K. Liu, D. Kulic, and J. Ichnowski, editors, *Proceedings of The 6th Conference on Robot Learning*, volume 205 of *Proceedings of Machine Learning Research*, pages 1157–1167. PMLR, 14–18 Dec 2023.
- [31] D. P. Kingma and J. Ba. Adam: A method for stochastic optimization. In Y. Bengio and Y. LeCun, editors, *3rd International Conference on Learning Representations, ICLR 2015, San Diego, CA, USA, May 7-9, 2015, Conference Track Proceedings*, 2015.
- [32] T. Howell, N. Gileadi, S. Tunyasuvunakool, K. Zakka, T. Erez, and Y. Tassa. Predictive Sampling: Real-time Behaviour Synthesis with MuJoCo. dec 2022.
- [33] O. Eberhard, J. Hollenstein, C. Pinneri, and G. Martius. Pink noise is all you need: Colored noise exploration in deep reinforcement learning. In *The Eleventh International Conference on Learning Representations*, 2023.
- [34] V. Caggiano, H. Wang, G. Durandau, M. Sartori, and V. Kumar. Myosuite: A contact-rich simulation suite for musculoskeletal motor control. In R. Firoozi, N. Mehr, E. Yel, R. Antonova, J. Bohg, M. Schwager, and M. J. Kochenderfer, editors, *Learning for Dynamics and Control Conference, L4DC 2022, 23-24 June 2022, Stanford University, Stanford, CA, USA*, volume 168 of *Proceedings of Machine Learning Research*, pages 492–507. PMLR, 2022.

- [35] H. Wang, V. Caggiano, G. Durandau, M. Sartori, and V. Kumar. Myosim: Fast and physiologically realistic mujoco models for musculoskeletal and exoskeletal studies. In *2022 International Conference on Robotics and Automation, ICRA 2022, Philadelphia, PA, USA, May 23-27, 2022*, pages 8104–8111. IEEE, 2022.
- [36] P. Schumacher, D. F. Haeufle, D. Büchler, S. Schmitt, and G. Martius. Dep-rl: Embodied exploration for reinforcement learning in overactuated and musculoskeletal systems. In *The Eleventh International Conference on Learning Representations (ICLR)*, May 2023.
- [37] J. Xu, V. Makoviychuk, Y. S. Narang, F. Ramos, W. Matusik, A. Garg, and M. Macklin. Accelerated policy learning with parallel differentiable simulation. In *The Tenth International Conference on Learning Representations, ICLR 2022, Virtual Event, April 25-29, 2022*. OpenReview.net, 2022.
- [38] I. Georgiev, K. Srinivasan, J. Xu, E. Heiden, and A. Garg. Adaptive horizon actor-critic for policy learning in contact-rich differentiable simulation. In *Forty-first International Conference on Machine Learning, ICML 2024, Vienna, Austria, July 21-27, 2024*. OpenReview.net, 2024.
- [39] M. Macklin. Warp: A high-performance python framework for gpu simulation and graphics. <https://github.com/nvidia/warp>, March 2022. NVIDIA GPU Technology Conference (GTC).
- [40] Y. Hu, J. Liu, A. Spielberg, J. B. Tenenbaum, W. T. Freeman, J. Wu, D. Rus, and W. Matusik. Chainqueen: A real-time differentiable physical simulator for soft robotics. In *2019 International conference on robotics and automation (ICRA)*, pages 6265–6271. IEEE, 2019.
- [41] M. Liu, G. Yang, S. Luo, and L. Shao. Softmac: Differentiable soft body simulation with forecast-based contact model and two-way coupling with articulated rigid bodies and clothes. In *2024 IEEE/RSJ International Conference on Intelligent Robots and Systems (IROS)*, pages 12008–12015. IEEE, 2024.
- [42] A. H. Taylor, S. Le Cleac’h, Z. Kolter, M. Schwager, and Z. Manchester. Dojo: A differentiable simulator for robotics. *arXiv preprint arXiv:2203.00806*, 2022.
- [43] R. Newbury, J. Collins, K. He, J. Pan, I. Posner, D. Howard, and A. Cosgun. A Review of Differentiable Simulators. *IEEE Access*, 12:97581–97604, 2024. ISSN 2169-3536.
- [44] E. Catto. Box2d is a 2d physics engine for games. 2018.
- [45] C. D. Freeman, E. Frey, A. Raichuk, S. Girgin, I. Mordatch, and O. Bachem. Brax - a differentiable physics engine for large scale rigid body simulation, 2021. URL <http://github.com/google/brax>.
- [46] K. Werling, D. Omens, J. Lee, I. Exarchos, and C. K. Liu. Fast and feature-complete differentiable physics engine for articulated rigid bodies with contact constraints. In *Robotics: Science and Systems*, 2021.
- [47] E. Catto et al. Modeling and solving constraints. In *Game Developers Conference*, 2009.
- [48] Y. Hu, T.-M. Li, L. Anderson, J. Ragan-Kelley, and F. Durand. Taichi: a language for high-performance computation on spatially sparse data structures. *ACM Transactions on Graphics (TOG)*, 38(6):201, 2019.
- [49] E. Heiden, D. Millard, E. Coumans, Y. Sheng, and G. S. Sukhatme. NeuralSim: Augmenting differentiable simulators with neural networks. In *Proceedings of the IEEE International Conference on Robotics and Automation (ICRA)*, 2021.
- [50] G. Yang, S. Luo, Y. Feng, Z. Sun, C. Tie, and L. Shao. Jade: A differentiable physics engine for articulated rigid bodies with intersection-free frictional contact. In *2024 IEEE International Conference on Robotics and Automation (ICRA)*, pages 16915–16922. IEEE, 2024.
- [51] D. M. Kaufman, S. Sueda, D. L. James, and D. K. Pai. Staggered projections for frictional contact in multibody systems. In *ACM SIGGRAPH Asia 2008 papers*, pages 1–11. 2008.
- [52] E. Todorov. A convex, smooth and invertible contact model for trajectory optimization. In *2011 IEEE International Conference on Robotics and Automation*, pages 1071–1076, May 2011. ISSN: 1050-4729.
- [53] E. Drumwright and D. A. Shell. Modeling contact friction and joint friction in dynamic robotic simulation using the principle of maximum dissipation. In *Algorithmic Foundations of Robotics IX: Selected Contributions of the Ninth International Workshop on the Algorithmic Foundations of Robotics*, pages 249–266. Springer, 2011.
- [54] R. Elandt, E. Drumwright, M. Sherman, and A. Ruina. A pressure field model for fast, robust approximation of net contact force and moment between nominally rigid objects. In *2019 IEEE/RSJ International Conference on Intelligent Robots and Systems (IROS)*, pages 8238–8245. IEEE, 2019.
- [55] T. Pang, H. T. Suh, L. Yang, and R. Tedrake. Global planning for contact-rich manipulation via local smoothing of quasi-dynamic contact models. *IEEE Transactions on robotics*, 39(6):4691–4711, 2023.
- [56] Y. Tassa and E. Todorov. Stochastic complementarity for local control of discontinuous dynamics. In *Robotics: Science and Systems*, volume 6, 2010.
- [57] J. C. Duchi, P. L. Bartlett, and M. J. Wainwright. Randomized smoothing for stochastic optimization. *SIAM Journal on Optimization*, 22(2):674–701, 2012.
- [58] H. J. T. Suh, T. Pang, and R. Tedrake. Bundled gradients through contact via randomized smoothing. *IEEE Robotics and Automation Letters*, 7(2):4000–4007, 2022.

- [59] K. Bouyarmane, A. Escande, F. Lamiriaux, and A. Kheddar. Potential field guide for humanoid multicontacts acyclic motion planning. In *2009 IEEE International Conference on Robotics and Automation*, pages 1165–1170. IEEE, 2009.
- [60] J. Xu, T.-K. J. Koo, and Z. Li. Sampling-based finger gaits planning for multifingered robotic hand. *Autonomous Robots*, 28(4):385–402, 2010.
- [61] Y. Zhang, D. Gopinath, Y. Ye, J. Hodgins, G. Turk, and J. Won. Simulation and retargeting of complex multi-character interactions. In *ACM SIGGRAPH 2023 Conference Proceedings*, pages 1–11, 2023.
- [62] O. Beker, N. Gürtler, J. Shi, A. R. Geist, A. Razmjoo, G. Martius, and S. Calinon. A smooth analytical formulation of collision detection and rigid body dynamics with contact. *arXiv preprint arXiv:2503.11736*, 2025.
- [63] DeepMind, I. Babuschkin, K. Baumli, A. Bell, S. Bhupatiraju, J. Bruce, P. Buchlovsky, D. Budden, T. Cai, A. Clark, I. Danihelka, A. Dedieu, C. Fantacci, J. Godwin, C. Jones, R. Hemsley, T. Hennigan, M. Hessel, S. Hou, S. Kapturowski, T. Keck, I. Kemaev, M. King, M. Kunesch, L. Martens, H. Merzic, V. Mikulik, T. Norman, G. Papamakarios, J. Quan, R. Ring, F. Ruiz, A. Sanchez, L. Sartran, R. Schneider, E. Sezener, S. Spencer, S. Srinivasan, M. Stanojević, W. Stokowiec, L. Wang, G. Zhou, and F. Viola. The DeepMind JAX Ecosystem, 2020. URL <http://github.com/google-deeppmind>.
- [64] C. Gumbsch, M. V. Butz, and G. Martius. Sparsely changing latent states for prediction and planning in partially observable domains. *Advances in Neural Information Processing Systems*, 34:17518–17531, 2021.
- [65] Y. Song, S. bae Kim, and D. Scaramuzza. Learning quadruped locomotion using differentiable simulation. In *8th Annual Conference on Robot Learning*, 2024.
- [66] J. Baumgarte. Stabilization of constraints and integrals of motion in dynamical systems. *Computer methods in applied mechanics and engineering*, 1(1):1–16, 1972.
- [67] P. Kidger and C. Garcia. Equinox: neural networks in JAX via callable PyTrees and filtered transformations. *Differentiable Programming workshop at Neural Information Processing Systems 2021*, 2021.
- [68] C. Tsitouras. Runge–kutta pairs of order 5 (4) satisfying only the first column simplifying assumption. *Computers & Mathematics with Applications*, 62(2):770–775, 2011.
- [69] J. R. Dormand and P. J. Prince. A family of embedded Runge–Kutta formulae. *J. Comp. Appl. Math*, 6: 19–26, 1980.
- [70] R. T. Q. Chen, Y. Rubanova, J. Bettencourt, and D. Duvenaud. Neural ordinary differential equations. *Advances in Neural Information Processing Systems*, 2018.
- [71] P. Stumm and A. Walther. New algorithms for optimal online checkpointing. *SIAM Journal on Scientific Computing*, 32(2):836–854, 2010. doi:10.1137/080742439.
- [72] Q. Wang, P. Moin, and G. Iaccarino. Minimal repetition dynamic checkpointing algorithm for unsteady adjoint calculation. *SIAM Journal on Scientific Computing*, 31(4):2549–2567, 2009. doi:10.1137/080727890.
- [73] A. R. Geist, J. Frey, M. Zhobro, A. Levina, and G. Martius. Learning with 3D rotations, a hitchhiker’s guide to SO(3). In *Proceedings of the 41st International Conference on Machine Learning*, volume 235 of *Proceedings of Machine Learning Research*, pages 15331–15350. PMLR, 21–27 Jul 2024.
- [74] R. Brégier. Deep regression on manifolds: a 3d rotation case study. In *2021 International Conference on 3D Vision (3DV)*, pages 166–174. IEEE, 2021.
- [75] C. C. Horuz, G. Kasenbacher, S. Higuchi, S. Kairat, J. Stoltz, M. Pesl, B. A. Moser, C. Linse, T. Martinetz, and S. Otte. The resurrection of the relu. *arXiv preprint arXiv:2505.22074*, 2025.

Supplementary Material for: Hard Contacts with Soft Gradients: Refining Differentiable Simulators for Learning and Control

A Related Work

Differentiable simulators are an active area of research spanning multiple fields of physics, including elastic object and fluids modeling [40, 39, 7, 41] and modeling rigid body collisions [6, 7, 42, 18] (see [43] for a recent overview). As outlined in Figure S1, we focus on robotics simulators involving hard contact collisions, with the hierarchical objectives of (i) accurately simulating dynamics, (ii) computing correct simulator gradients, and (iii) obtaining informative gradients between non-colliding objects.

Simulating contact dynamics. Commonly deployed robot simulators can be categorized according to their contact model into impulse-based [44, 45, 7], complementary-based [42, 46], and penalty-based [6] approaches. Due to their simplicity and speed, impulse-based simulators [47], such as those using DiffTaichi [48, 7], are widely used in game development but remain currently uncommon in robot controller synthesis. Complementary-based contact models compute constraint forces as a solution to a constrained optimization problem either in the form of a nonlinear-complementary problem (NCP) [42] or linear-complementary problem (LCP) [16, 15, 49, 50]. Exactly solving NCP is an NP-hard problem [51] that is considerably difficult to solve even approximately. The NCP formulation in Dojo is physically more accurate than LCP formulations [42], but lacks support for parallel computation limiting its utility for controller synthesis. That said, it is currently not clear which complementary formulation is best suited for robotics.

To improve computational efficiency, MuJoCo [6, 12] reformulates the complementary constraint problem as a convex optimization problem. This reformulation builds on prior work on complementarity-free approaches [52, 53]. A detailed description of MuJoCo is provided in Sec. B.1. Briefly, contact forces are computed by solving a global optimization problem, in which the ability of a constraint to generate force is modulated by the geometric penetration depth at the contact interface. As an alternative, Drake [16] also adopts a soft patch contact model [54, 55]. In turn, these approaches to contact resolution soften the dynamics.

Differentiating through contacts. The choice of contact model has significant implications on the differentiability of the simulator. If complementary-based solvers exactly compute hard contact forces, then the resulting jumps in the dynamics aggravate gradient computation. Hence, recent literature on differentiating through complementary-based solvers propose analytical reformulations of the dynamics, e.g. based on the implicit function theorem [46, 42], or resort to randomized smoothing [56, 57, 58, 59, 60]. While differing in their computational cost, these approaches to smoothing have been shown to be empirically equivalent [55, 8].

While the dynamics of penalty-based simulators are inherently smooth, gradient inaccuracies introduced by time discretization grow with both contact stiffness and integration step size. Prior work has attributed this problem to time-of-impact discretization errors [7, 8]. As a result, accurately simulating near-rigid contacts within penalty-based frameworks requires significantly smaller integration step sizes, which limits their practicality for robot controller synthesis. In this work, we propose an alternative direction: adaptively integrating compliant simulators.

Goal 1: Realistic simulation

Solution 1: Exact contact solving	Solution 2: Compliant contacts with stiff settings
--------------------------------------	--



Goal 2: Accurate gradients

Solution 1: Randomized smoothing	Solution 3: Finite differences
Solution 2: Analytic smoothing	Solution 4 (ours): Adaptive integration



Goal 3: Contact invariance

Solution 1: Inter-body distances	Contact-invariant optimization
Solution 2 (ours): Contacts from distance	Straight-through estimation

Figure S1: Overview on hierarchical goals that need to be accomplished to use simulator gradients for robot controller synthesis.

Contact-invariant optimization. To guide an optimizer toward using body collisions for task facilitation, recent works in controller synthesis and path planning incorporate inter-body distances into the optimization objective. In RL, [61] added inter-point distances to rewards using a softmax function. Alternatively, the algorithms in MuJoCo MPC [32] rely on inter-point distances combined with trajectory samples establishing contact to inform the optimization. However, depending on the task at hand, setting up distance-based loss terms to inform an optimizer about the necessity for specific object collisions can quickly become cumbersome. As an alternative approach, Mordatch et al. [10] proposed the framework of “*contact-invariant optimization*” (CIO) in which a simulation is adjusted to also apply contact forces between non-colliding bodies. While the simulation can apply non-physical contact forces, the optimization is encouraged through the addition of several loss terms to minimize the usage of these forces. In [9], CIO was extended to in-hand manipulation of objects. Our proposed extension of *contacts from distance* (CFD) is inspired by CIO. Yet, while CIO applies artificial contact forces in the forward simulation, CFD resorts to the straight-through-trick to only exert contact forces in a simulation that is solely used for gradient computation. In turn, CFD does not require the addition of regularization terms to a loss when used for planning. Recently, [62] proposed soft signed distance fields as an alternative geometry representation, while also adjusting collision detection and contact force computation to be inherently soft. This approach which routes at the geometry level of robot simulation can be seen as an alternative avenue towards CIO.

Straight-through estimation. The use of the straight-through-trick in CFD is inspired by a plethora of works in robotics and beyond. The code underlying the straight-through-trick is reported in JAX [63] documentation under the collective heading of *straight-through estimation*. Straight-through estimation has been used in [64], where the backward pass of a Heaviside function is replaced with an identity function to obtain sparse RNNs for model-based RL. Horuz et al. [75] demonstrate that using a ReLu activation with a custom backward function rivals smooth ReLu surrogates. Recently, [65] replaced simulator dynamics obtained from IsaacGym [17] with single-rigid body dynamics for the gradient computation in the backward pass. This approach is closely related to our work, but unlike CFD, [17] does not utilize the forward pass simulation in the backward pass, limiting its utility for complex control synthesis tasks and system identification.

B Method Details

B.1 Contact force computation in MuJoCo

A detailed description of MuJoCo is given in its documentation², here we merely provide a digestible summary of the key equations. Through the Newton-Euler equations of the unconstrained system (1), one can determine the acceleration produced by a specific generalized force, and utilizing the collision detector along with geometrical data, we can identify the location of contact forces exerted by body points. This leaves us with the question on the direction and magnitude of constraint forces. MuJoCo finds an approximate answer to this question by resorting to Gauss principle [19, 20] which states that nature chooses the acceleration of rigid-body systems such that the weighted square norm $\|J^\top f\|_M^2$ is minimized while all constraints are met exactly. MuJoCo deploys softened versions of Gauss principle and Baumgarte stabilization, reading

$$\begin{aligned}
 (\dot{v}, \dot{\omega}) = \arg \min_{(x, y)} & \underbrace{\|x - M^{-1}(\tau - c)\|_M^2}_{\text{Inspired by Gauss' principle}} + \underbrace{\|y - a_{\text{ref}}\|_{R^{-1}}^{\text{Huber}}}_{\text{Inspired by Baumgarte stabilization}} \\
 \text{subject to} & \quad J_{\mathcal{E}}x - y_{\mathcal{E}} = 0, \quad J_{\mathcal{F}}x - y_{\mathcal{F}} = 0, \quad J_{\mathcal{C}}x - y_{\mathcal{C}} \in \mathcal{K}^*
 \end{aligned} \tag{S1}$$

with the index sets for equality, friction, and contact constraints $\mathcal{E}, \mathcal{F}, \mathcal{C}$, the friction cone (dual) \mathcal{K}^* , the regularizer $R > 0$, and $\|\cdot\|^{\text{Huber}}$ denoting the Huber norm. The reference acceleration a_{ref} denotes the solver’s target for the constraint space acceleration $\dot{\omega}$. Drawing inspiration from Baumgarte

²<https://mujoco.readthedocs.io/en/stable/computation/index.html>

stabilization [66], MuJoCo chooses a_{ref} as the dynamics of a spring-damper system, writing

$$a_{\text{ref},i} = -b_i(Jv)_i - k_i r_i = -\frac{2}{(d_w \cdot t_c)}(Jv)_i - \frac{d(r_i)}{(d_w^2 \cdot t_c^2 \cdot \phi_d^2)} r_i, \quad (\text{S2})$$

whose dynamics are determined by the impedance $d(r)$, and the *solref* parameters consisting of the time constant t_c and the damping ratio ϕ_d . The *impedance* $d(r)$ is the central function for determining constraint forces (such as contact forces). As illustrated in Figure 3, the impedance $d \in (0, 1)$ is a function of the constraint violation r and is specified by the *solimp* parameters (d_o, d_w, w , midpoint, power) which determine its shape as a polynomial spline. MuJoCo’s documentation refers to the *impedance* as a “constraints ability to generate force” as it not only determines a_{ref} , but also directly weights the cost for applying constraint forces in Eq. (S1) via R , which is computed as

$$R = \frac{1 - d_i}{d_i} \hat{A}_{ii}, \quad (\text{S3})$$

where \hat{A}_{ii} denotes an approximation to the diagonal entries of the inverse inertia in constraint space $A_{ii} = JM^{-1}J^\top$. In turn, the constraint is hard if $R \rightarrow 0$, and more soft for larger R , approaching an infinitely soft (i.e. non-existent) constraint in the limit $R \rightarrow \infty$. As outlined in Appendix B.1, MuJoCo transforms Eq. (S1) into a convex problem that is solved efficiently by an exact Newton method.

If \mathcal{K}^* solely contains pyramidal or elliptic cone constraints, then the constrained optimization problem can be reduced to the convex problem

$$\dot{v} = \arg \min_x \|x - M^{-1}(\tau - c)\|_M^2 + s(Jx - a_{\text{ref}}). \quad (\text{S4})$$

where the analytical function $s(\cdot)$ acts as a soft constraint penalty. By default, MuJoCo solves (S4) using an exact Newton method. While we do not delve into the inner workings of MuJoCo’s constraint solver, the reader should keep in mind that the number of solver iterations and its error tolerance affect the stability of the simulation.

B.2 ODE differentiation in Diffrax

Diffrax: Numerical integration with JAX The ODE solved by the Mujoco simulator can be written as

$$x(0) = x_0 \quad \dot{x}(t) = F_\theta(t, x(t)) \quad (\text{S5})$$

where θ incorporates all model parameters and x is the full state of the system.

In this work, we resort to the Diffrax library [25, 67] for numerical integration in Jax to solve the above ODE. This powerful library provides efficient implementations of many fixed and adaptive timestep solvers [68, 69]. It also allows easily switching between different modes for backpropagation: Discretize-then-optimize (also referred to as unrolling) and optimize-then-discretize (also referred to as backsolving) [70, 25]. Overall, the choice of solver, stepsize controller and differentiation technique is typically application-dependent. Hence, we implement the general Diffrax integrator as an easy-to-use alternative for the existing fixed-stepsize integrators in MJX, offering the full flexibility of the Diffrax library to the user. Notably, we adjust the Diffrax solvers to accommodate for exact integration of quaternions and stateful actuators, similar to the Runge-Kutta implementation of MJX, which can help to reduce the number of required integration steps.

Discretize-then-optimize. The first notable differentiation mode is discretize-then-optimize. It is the result of discretizing the forward ODE with a numerical integrator and then computing the gradients of the discretized forward ODE by unrolling the computation graph. This approach aligns with the paradigm of differentiable programming used in autodifferentiation libraries such as JAX, hence this is also the approach taken in standard MJX. The problem here is that the memory requirements scale linearly with the number of solver steps. For many applications this is a serious

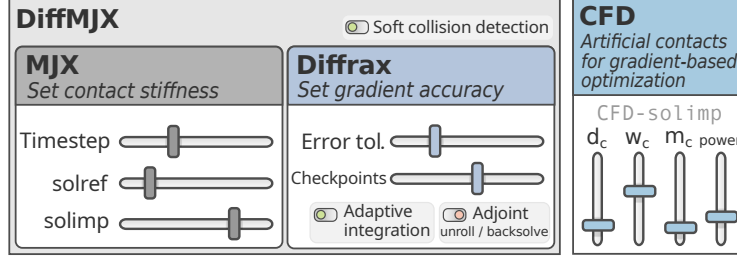


Figure S2: **DiffMJX and CFD add tuning knobs to MJX’s gradient computation.** DiffMJX adds support for adaptive integration atop MJX. The integrator’s error tolerances allows to trade computational speed for improved gradient accuracy. The number of checkpointing steps trades computation speed for improved GPU memory consumption. CFD adds parameters that set the distance and magnitude at which artificial contact forces are applied in the gradient computation.

bottleneck in standard MJX, and the problem is exacerbated when relying on adaptive integration, as it typically involves storing even more substeps. Fortunately, DiffMJX already implements an optimal gradient checkpointing scheme that allows reducing memory requirements from $O(n)$ to $O(1)$ in exchange for increasing runtime from $O(n)$ to $O(n \log n)$, where n is the maximum number of solver steps.

Another potential issue is that discretize-then-optimize inherently computes gradients of the discretized dynamics, rather than the true continuous dynamics. This can lead to interesting failure cases in which even in the limit of the stepsize going to zero, the computed gradient is different from the true gradient of the continuous dynamics. This is the result of the basic fact that the convergence of a parameterized function (the discretized ODE) to a limit (the continuous ODE) does not imply the convergence of its gradient. Note that this is not a mere mathematical corner case, instead it is the underlying reason for time-of-impact oscillations as described in Figure 4 and [7, 8].

Optimize-then-discretize. Fixing this requires (approximately) computing the gradients of the true continuous forward ODE. This is achieved by analytically computing the gradient as the solution to the continuous adjoint equations. Assuming a loss $L = L(x(T))$ only on the final state w.l.o.g., the continuous adjoint equations [25, Theorem 5.2] can be written as:

$$a_x(T) = \frac{dL}{dx(T)} \quad \dot{a}_x(t) = -a_x(t)^\top \frac{\partial F_\theta}{\partial x}(t, x(t)) \quad (\text{S6})$$

$$a_\theta(T) = 0 \quad \dot{a}_\theta(t) = -a_x(t)^\top \frac{\partial F_\theta}{\partial \theta}(t, x(t)) \quad (\text{S7})$$

Solving these using any numerical solver on the backward pass, as offered readily by the DiffMJX library, yields the desired gradients $\frac{dL}{dx(t)} = a_x(t)$ and $\frac{dL}{d\theta} = a_\theta(0)$.

This approach is called “optimize-then-discretize” or BacksolveAdjoint in DiffMJX. Note also that the memory requirements can again be reduced to constant in the number of solver steps, by solving the forward ODE “backwards in time” together with the adjoint ODE. Optimize-then-discretize, in contrast to unrolling, allows to directly specify tolerances on the error in the gradients.

One of the intuitive potential benefits of optimize-then-discretize is that the adaptive stepsize controller for solving the adjoint ODE now has the ability to adapt the stepsize when computing the adjoint derivatives, rather than being constrained to unrolling the steps that were taken during the forward solve. However, in practice it is typically the case that the forward ODE and the adjoint ODE are stiff “in the same regions”, i.e. the state derivative changes quickly when the state itself changes quickly. Hence, when unrolling the forward solve, the steps are already small in the regions where the adjoint ODE is also stiff. Therefore it typically suffices to use the less complicated discretize-then-optimize, which has a less complex computational graph and therefore comes with lower compilation times. The above explanation of course only holds when the forward ODE and the adjoint ODE “match”;

when modifying the adjoint ODE (as will be discussed in the following section) it may be beneficial to use optimize-then-discretize.

B.3 Contacts from distance with the straight-through-trick

To implement contacts-from-distance only on the backward pass, we use the straight-through trick on the ODE level:

$$\dot{x}(t) = \text{sg}(F_\theta(t, x(t))) + \tilde{F}_\theta(t, x(t)) - \text{sg}(\tilde{F}_\theta(t, x(t))), \quad (\text{S8})$$

where sg is the stop-gradient operator. Here \tilde{F} would be obtained by modifying the reference acceleration and impedance as described in Figure 6. In code this reads as:

```
1 from jax.lax import stop_gradient
2 def forward(m: Model, d: Data) -> Data:
3     d_mjx = _forward(m, d, cfd=False) # Compute system acceleration without CFD
4     d_cfd = _forward(m, d, cfd=True)  # Compute system acceleration using CFD
5     grad_replace_fn = lambda x_mjx, x_cfd: stop_gradient(x_mjx) + x_cfd - stop_gradient(x_cfd)
6     return jax.tree.map(grad_replace_fn, d_mjx, d_cfd) # Reroute gradient computation
```

This effectively means that on the forward pass, we use $F_\theta(t, x(t))$, whereas on backward we use $\frac{\partial \tilde{F}_\theta}{\partial(x, \theta)}(t, x(t))$. Crucially, the derivatives are evaluated at the unmodified forward trajectory $x(t)$. Differentiation still works readily with both ODE differentiation techniques described in the previous section. In discretize-then-optimize, automatic differentiation automatically uses the vector-jacobian-products derived from \tilde{F}_θ instead of F_θ . In optimize-then-discretize, with the straight-through-trick applied to F , we replace the vector-jacobian-products in the adjoint equations Eq. (S6) as follows

$$\tilde{a}_x(T) = \frac{dL}{dx(T)} \quad \dot{\tilde{a}}_x(t) = -\tilde{a}_x(t)^\top \frac{\partial \tilde{F}_\theta}{\partial x}(t, x(t)) \quad (\text{S9})$$

$$\tilde{a}_\theta(T) = 0 \quad \dot{\tilde{a}}_\theta(t) = -\tilde{a}_x(t)^\top \frac{\partial \tilde{F}_\theta}{\partial \theta}(t, x(t)). \quad (\text{S10})$$

Solving these altered adjoint equations gives replacements for the respective gradients, which in our case incorporate gradient information on contacts from distance. Again, this approach does not require any additional implementation effort, as the straight-through-trick allows to just use the existing Diffrax implementation of optimize-then-discretize.

Optimize-then-discretize vs Discretize-then-optimize in the presence of CFD. As discussed in the previous section, adding contacts from distance may change the preferred choice of gradient computation, as the forward and adjoint ODE may have different stiffness values in different regions.

To illustrate this, we again consider a version of the billiard-toy example from Figure 8. This time, we turn gravity off and disable the table-ball contacts to isolate the ball-ball contact, which means that the ODE is linear before and after the collision. We again compute the loss and gradient over a range of initial parameters, the results are reported in Figure S3. As before, we observe that with the DiffMJX adaptive integrator, we get well-behaved gradients, but the gradient becomes zero when the two balls do not collide.

Now, we activate the CFD mechanism and repeat the experiment. In this case, the gradient show oscillations due to the different stiffness settings of the forward and adjoint ODE: The solver for the forward ODE takes very large steps when no ball-ball collision happens, but the adjoint ODE incorporates the collision signal and hence is stiff. Simply unrolling the forward integration therefore makes a discretization error, resulting in the oscillations. Note, that we did not observe this phenomenon in Figure 8, as this experiment includes ball-table collisions which cause the adaptive solver of the forward ODE to take small steps even when no ball-ball collision is happening. The solution is to use optimize-then-discretize. Here, the adaptive solver for the adjoint ODE can select stepsizes according to the stiffness of the adjoint ODE. This is also confirmed by the results in Figure S3 (right).

This experiments highlights an extreme corner case, and we did not observe issues in our other experiments when using discretize-then-optimize with CFD, as we typically do not have such extreme

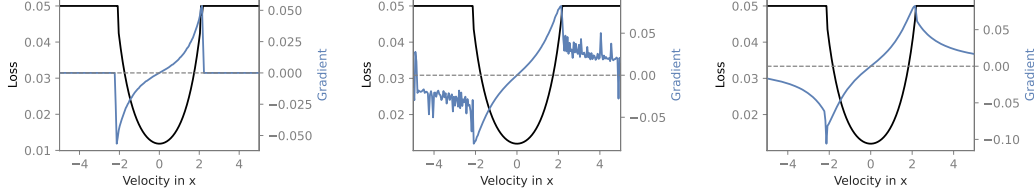


Figure S3: Optimize-then-discretize vs discretize-then-optimize in the presence of contacts-from-distance. Results are for a reduced billiard example as in Figure 8, but without table-ball contacts and gravity. **Left:** DiffMJX adaptive integration results in well-behaved gradients, but gradient is zero if objects do not collide. **Middle:** Using CFD with *discretize-then-optimize* results in small gradient oscillations. The adaptive integrator selects large stepsizes as no contacts are happening (forward ODE is non-stiff), whereas in the gradient computation the CFD are added (adjoint ODE is stiff). In turn, unrolling the large stepsizes cause discretization errors. Note that this phenomenon persists no matter how low the tolerance of the forward ODE solver is set, as the stepsize controller is completely unaware of the CFD mechanism that is only used in the gradient computation. **Right:** Using *optimize-then-discretize* allows the solver for the adjoint ODE to select small stepsizes when the adjoint ODE is stiff due to CFD. This fixes the gradient oscillations.

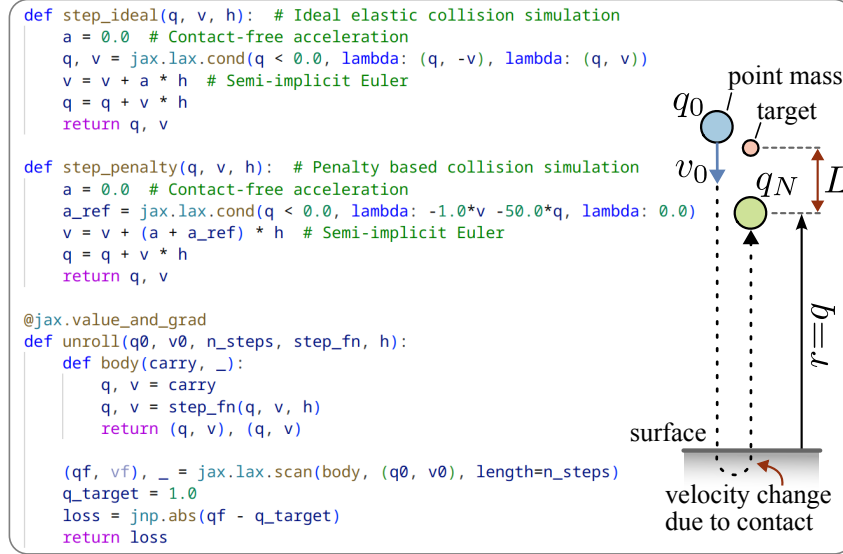


Figure S4: **Jax code for minimal collision simulation.** The code simulates a minimal version of a penalty-based or ideal-elastic simulator and is used in Sec. 4 to illustrate the TOI discretization errors as shown in Figure 4.

variations of the stiffness in the forward ODE. However, we believe it is beneficial to be aware of this potential caveat and how one can resolve it with the tools available in DiffMJX.

C Evaluation details and further experiments

C.1 Gradient analysis of MJX

In Sec. 4, the time discretization errors arising in penalty-based simulators are first illustrated on a minimal toy example. The code to generate this toy example is shown in Figure S4. After illustrating on this toy example that time discretization errors can be mitigated by reducing the stepsize, it is shown in Figure 5 that these errors also occur in MuJoCo. Figure S5 is an extended version of Figure 5 containing all of MuJoCo’s basic shape primitives.

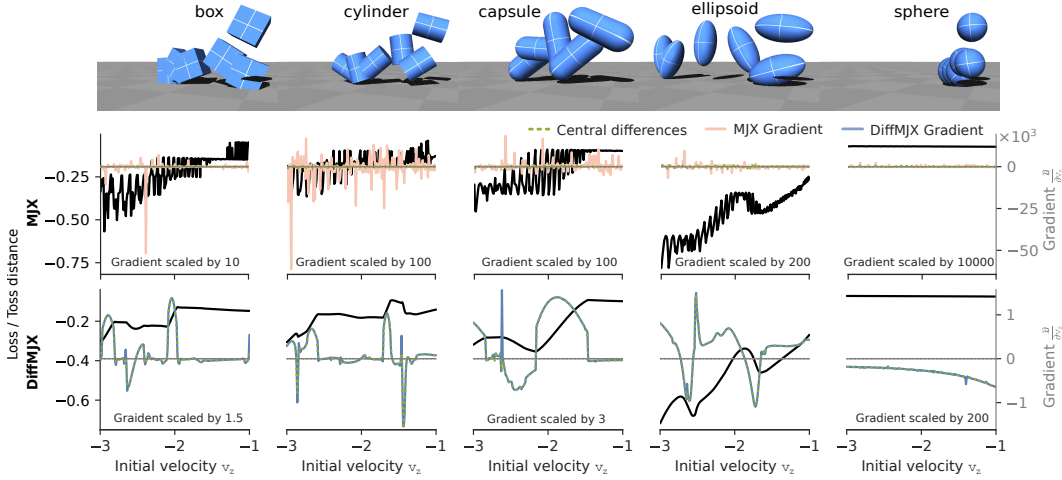


Figure S5: Simulation of geometric primitives thrown onto a surface using MJX or DiffMJX. Contacts at default stepsize 0.002 s, $\text{solref}=[0.005 \ 1.0]$, and $\text{solimp}=[0.0 \ 0.95 \ 0.001 \ 0.5 \ 2]$ cause MJX’s gradients of the toss distance to deviate significantly from central difference gradients, while DiffMJX maintains close agreement.

Figure S6 shows the error vs runtime trade-off for different integrators in MJX and DiffMJX. We observe that in the case of the cube toss, the adaptive integrators can severely reduce the runtime required to achieve gradients with low error.

C.2 System identification experiments

Contactnet dataset The contactnet dataset³ consists of 550 trajectories of an acrylic cube that has been repeatedly tossed onto a wooden table. As reported in [26, 28], data has been collected at 1480 Hz and the cube’s physical parameters amount to a side length of 10 cm, mass of 0.37 kg, inertia of 0.0081 kg m², a friction coefficient of 0.18, and restitution of 0.125.

Training setup The trajectories are split into segments of length five. In the supervised train loop, given a trajectory segment’s initial state, each simulator is unrolled for four steps. Subsequently, an mean square error (MSE) loss between the segment’s states and predicted states is computed. Before being fed to the loss function, each state’s quaternion is converted to a rotation matrix to avoid representation singularities negatively affecting training [73, 74]. For adaptive integration, DiffMJX is set to use “RecursiveCheckpointing” and a 5th order explicit Runge–Kutta method (“Tsits5” in DiffraX) with PID error tolerances of 1e-5. We use the Adam [31] implementation from the Optax library [63] for gradient-based optimization with parameters $[b1 = 0.5, b2 = 0.9, \text{eps} = 1 \text{e-}6]$. MuJoCo’s parameter are set to a timestep of 0.006767 s (the data collection sampling time), $\text{iterations}=4$ (contact solver iterations), $\text{ls_iterations}=10$ (solver steps), $\text{tolerance}=1\text{e-}8$, $\text{impratio}=1.0$, $\text{solref}=[0.02 \ 1]$, $\text{solimp}=[0.05 \ 0.95 \ 0.01 \ 0.5 \ 2]$, and friction $\text{solimp}=[0.4 \ 0.01 \ 0.1]$. The cube’s mass is set to the reported groundtruth value and its inertia is computed by MuJoCo’s default equal density approximation. DiffMJX uses the same MuJoCo settings with the exception of $\text{iterations}=2$ (adaptive integration does not require as many solver iterations). The CFD impedance function is set $[0.0, 0.01, 0.01, 1.0, 4.0]$ that is $d_c = 0.01$, $d_0 = 0$ with $w_c = 1 \text{ m}$.

C.2.1 Identification of additional MuJoCo parameters

In this section, we extend the experiment from Sec. 5.1 and use DiffMJX to estimate MuJoCo’s simulation parameters alongside the cube’s side length. In these experiments, the same setup is used for DiffMJX as detailed in the previous section. In comparison to the experiment in Sec. 5.1, the

³<https://github.com/DAIRLab/contact-nets>

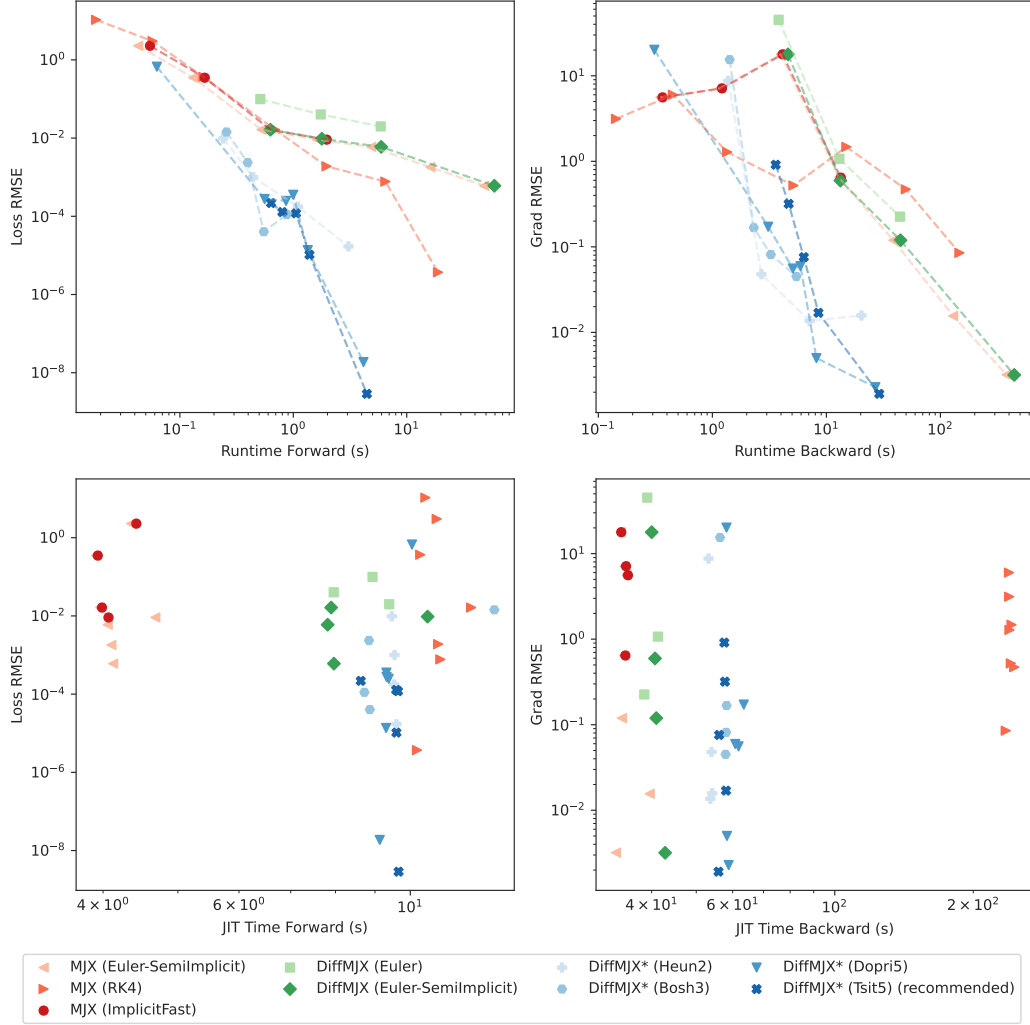


Figure S6: Error of loss and gradient vs runtime and compilation time for different integrators. The loss and gradient are computed for the cube toss shown in Fig. S5 at an initial velocity of $v_x = -2.0$ with contact settings `solref=[0.005 1.0]` and `solimp=[0.0 0.95 0.001 0.5 2]`. The rollout is also visualized at the top of this figure. The ground-truth gradients are computed from finite-differences using an adaptive solver with very low tolerance (10^{-12}) to simulate the rollout. Standard fixed-stepsize MJX integrators have red colors, fixed-stepsize integrators in Difffrax have green color, and adaptive-stepsize integrators in Difffrax have blue color (also marked by *). For adaptive stepsize control we use the Difffrax PID controller with $P = 0.2$, $I = 0.4$, $D = 0.0$, as recommended for stiff ODEs. We observe that the pareto-front of adaptive solvers is shifted, allowing lower loss and gradient errors with less runtime. The best-performing solver is the Tsit5 solver [68], which is a 5th order explicit Runge–Kutta method with an embedded 4th order method for adaptive step sizing. This is also the default solver used in other experiments.

integration error tolerance is increased to $1e-4$ to reduce computation time. Moreover, the parameters are constrained using either a softplus function or a softclip function where the softening hyperparameter has been carefully tuned. While the models are trained on an MSE between trajectory segments, we evaluate the model on the “trajectory error” being the mean absolute error between the first forty trajectories in the dataset and DiffMJX’s trajectory prediction. In these experiments, DiffMJX estimates the following parameters simultaneously:

- sidelength as also estimated in Sec. 5.1,
- mass from which MuJoCo automatically computes the cube’s inertia,
- solref parameters (time constant t_c , damping ratio ϕ_d) determining the constraint stiffness,
- solimp parameters determining the constraint’s ability to generate force,
- friction parameters determining the extend of the contact friction cone.

In total, we conduct two additional experiments with the Contactnets dataset:

Starting from pre-tuned initial conditions: The optimization is started from the same pre-tuned initial conditions as used in Sec. 5.1. The prediction horizon is set to $N = 10$. The training results are shown in Figure S7 (Center). Each model requires around 10 seconds of computation time per gradient step.

Starting from random initial conditions: The optimization is started with random initial parameters. The prediction horizon is set to $N = 4$ such that the majority of runs require around 5 seconds for a gradient step. The training results are shown in Figure S7 (Bottom).

In both experiments, the trajectory error remains above 0.25. As noted by Parmar et al. [27], the dynamics of a hard cube exhibit a degree of chaotic behavior. Consequently, small variations in initial conditions – potentially arising from sensor noise or external disturbances such as wind – can substantially alter the cube’s trajectory after one of its corners hits the table. Nevertheless, the reduction in trajectory error from approximately 0.32 to 0.26 results in the simulated cube notably more closely matching the real-world data, as shown in Figure S7.

In both experiments, the sidelengths of most models converged closely to the groundtruth. Albeit a small offset to the groundtruth sidelength remains for the majority of the runs.

C.3 MPC experiment

Experimental setup. The MyoHand and MyoArm collision parameters are set to `solref=[0.02 1.0]`, and `solimp=[0.0 0.95 0.001 0.5 2]`, the racket collision parameters are set to `solref=[-100000 0]` for elastic collision. When using CFD, we set `solimp=[0.1 0.95 0.001 0.5 2]` and use `solimp-CFD=[0.0 0.1 1.0 1.0 4]`. The timestep of the simulation is set to 0.0025, the constraint solver is the Newton solver with 4 iterations and 16 linesearch iterations. All models use our refinements for improving differentiability of MuJoCo’s collision detector.

All MPC experiments are performed on a NVIDIA GeForce RTX 3060. In the in-hand manipulation task the runtimes for the gradient-based MPC are 2.9h (+2.2h JIT) without CFD and 6.4h (+2.1h JIT) with CFD. The sampling with 1024 samples takes 35min (+3min JIT). In the bionic tennis task, the runtimes for the gradient-based MPC are 9.7h (+1.2h JIT) with CFD. The sampling based MPC runs for 1.4h with 2048 samples.

Note, that we did not optimize any of the methods for speed in this experiment, i.e. in baoding with gradients the task was solved after less than half the total timesteps. The main point here is that we can solve the challenging task using a purely gradient-based method that scales to high-dimensional systems. The large runtime of the gradient-based approach is mainly due to inefficient automatic differentiation of the MJX simulation, which remains the strongest limitation on gradient-based approaches at this point. One potential improvement could be to implement implicit differentiation of the constraint solver in MJX, which could allow for much more efficient gradient computation.

Before training:



After training (starting from pre-tuned initial conditions):

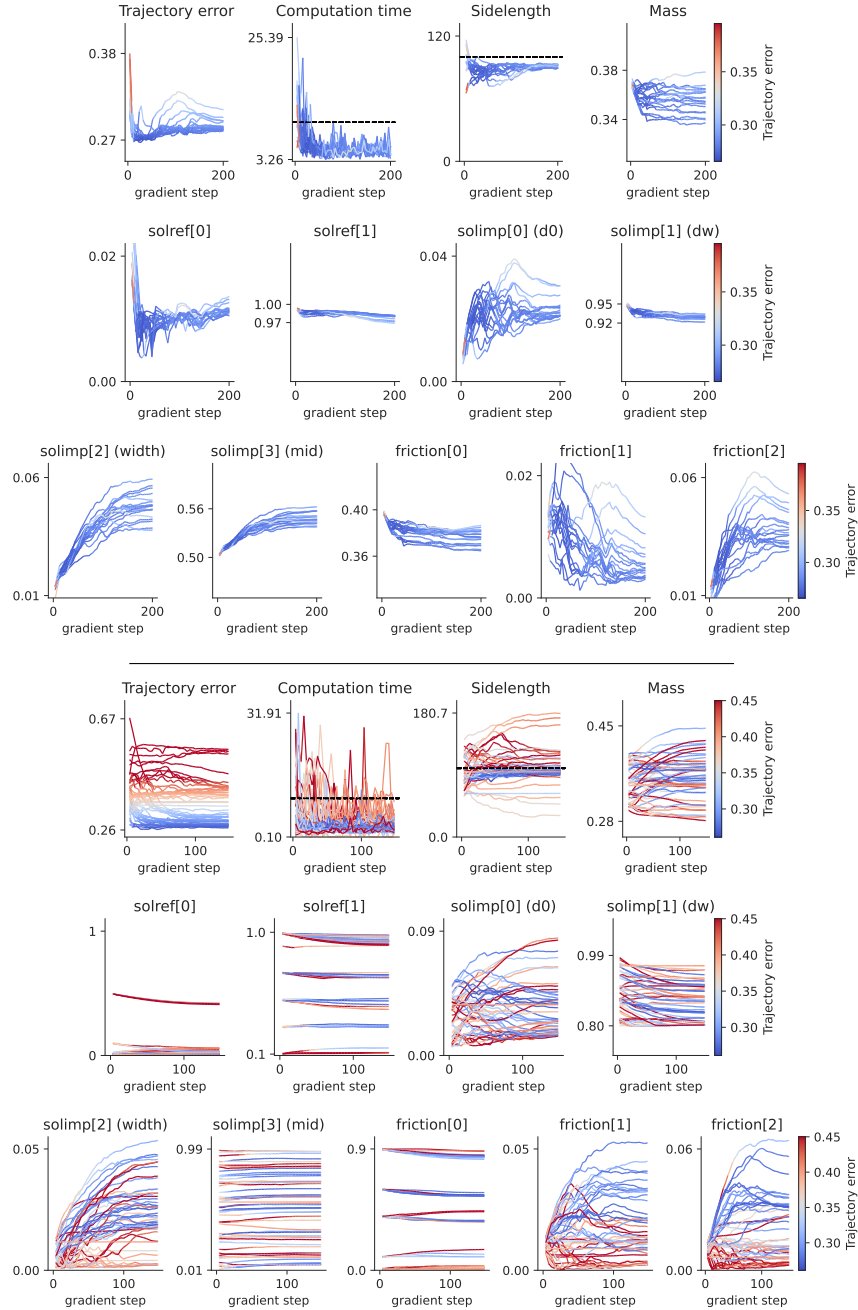


Figure S7: **Top:** Example trajectory predictions of DiffMJX before/after training. **Center:** Identification of MuJoCo parameters with DiffMJX on Contactnets cube toss dataset starting from pre-tuned initial conditions. **Bottom:** Identification starting from random initial parameters. The cube's geometry has a significant effect on the time of impact such that the optimization converges to a sidelength close to 100 mm to reduce the train loss. The effect of other model parameters on the system dynamics is more inter-twined. For example, a too large mass resulting in larger penetrations during impact can be compensated by increasing the constraint stiffness via `solref[0]` or `solimp[0]`.